Renewable resources derived hyperbranched polyurethane/silane-modified graphene oxide nanocomposite

Highlight

The current chapter describes the formation of nanocomposite of renewable resource derived hyperbranched polyurethane (HPU) with a silane-modified graphene oxide nanomaterial. An *in situ* polymerization technique was used to fabricate the nanocomposites with three different loadings (0.5, 1.0 and 2.0 wt%) of the 3-aminopropyltriethoxysilane-functionalized graphene oxide nanosheet (Si-GO). The nanomaterial and fabricated nanocomposite were characterized by various spectroscopic, microscopic and analytical techniques. Significant enhancements of mechanical properties like tensile strength (~247%), elongation at break (~206%) and toughness (~339%) were observed upon incorporation of very low amount (upto 2 wt%) of nanomaterial in HPU matrix. The nanocomposite exhibited excellent self healing ability under microwave (within 50-60s at 450 W) and sunlight (within 4-6 min under 10^6 lux) exposure with high efficiency (upto 100%). The surface of the nanocomposite also displayed inherent hydrophobicity (water contact angles upto 105°) without any additional surface modification. The development of such high performance polymeric materials with inherent smart features promises well for versatile applications including self healing and self cleaning materials.

Excerpts of this chapter are published in

Bayan, R. and Karak, N. Bio-derived aliphatic hyperbranched polyurethane nanocomposites with inherent self healing tendency and surface hydrophobicity: Towards creating high performance smart materials. *Composites Part A: Applied Science and Manufacturing*, 110:142-153, 2018.

4.1. Introduction

The previous chapter (Chapter 3) explored the potential of rGO based carbon nanomaterial as a reinforcing agent for renewable resource derived HPU towards property enhancement and prospective applications as shape memory materials. In this context, it is noteworthy to mention that PU with target-specific composition can be fine-tuned for making high performance materials with such smart attributes [1]. The development of smart polymers is gaining significant interest in the scientific community over the last decade [2, 3]. Such polymers are known to respond to a stimulus as desired and show unusual qualities [1-3]. In this context, self healing polymers (SHPs) and self cleaning polymers (SCPs) are the neo-generation smart materials that are attracting copious attention for utilization in various applications, as such polymers reduce energy consumption and minimize resource use and waste [2]. SHPs are a class of smart polymers which have the ability to repair the damage caused by mechanical strain over time [4], whereas SCPs are a special class of smart polymers that keep the surface free from dirt and mire [5]. Over the last few years, there are huge developments in polymeric materials, especially related to self healing and self cleaning properties [6-10]. However, the major challenge is to combine these properties in a single material. One of the key impediments in this regard is the structural incompatibility of such materials. The structural features of SHPs require high polymeric chain mobility and chain diffusion [4], while SCPs necessitate hydrophobic/hydrophilic surface for dirt removal [5]. Therefore, tuning of such properties in a single polymeric material is of utmost interest.

HPUs in particular, owing to their myriad properties are good choice for fabrication of such smart polymers [2]. At its core, intrinsic self healing is driven by dynamics of polymer chain and supramolecular assembly at molecular scale [4]. In this regard, HPU possessing an inherent blend of hard and soft segments that enable chain mobility and diffusion, may hold the key for achieving self healing ability. At the same time, self cleaning ability is driven by low surface energy of material and presence of geometrical microstructures, which ultimately imparts hydrophobicity [5]. As such the combination of a suitable HPU and surface morphological changes created by incorporation of suitable nanomaterial, may introduce hydrophobic character required for introducing self cleaning property.

As discussed in Chapter 1, graphene and its variants are the choice of material for imbibing or improving smart property in polymer matrices, due to their superior mechanical, thermal and electrical properties. There is abundant literature on graphene based PUNCs with various smart attribute. Han and Chun reported the preparation of PUNC

with functionalized graphene and its shape memory effects [11]. Kim et al. reported synthesis of PU/graphene nanocomposite with self healing ability [12]. Thus, development of HPUNCs with suitable graphene-based nanomaterial may realize the vision of having self healing and self cleaning property in the same material.

In this perspective, the fabrication of renewable resources based HPUNC with silane-functionalized GO (Si-GO) nanomaterial was reported. Different compositions of the nanocomposite with respect to loading of Si-GO were prepared by *in situ* polymerization technique. The nanocomposite was investigated for mechanical, thermal and chemical properties. The nanocomposite was screened for self healing and self cleaning attributes.

4.2. Experimental

4.2.1. Materials

PCL, IPDI, MGE, COMP, xylene and THF were used for the preparation of HPUNC. Molecular sieves were used to store the solvents. All these chemical possess the same grade and specifications as described in Chapter 2 (Section 2.2.1). Graphite, potassium permanganate ($KMnO_4$), hydrogen peroxide (H_2O_2), concentrated sulphuric acid (conc. H_2SO_4) and dilute hydrochloric acid (dil. HCl) were used for the preparation of GO. All these chemical possess the same grade and specifications as mentioned in Chapter 3 (Section 3.2.1).

3-Aminopropyltriethoxysilane (APTES) was used for functionalization of GO. It is a colorless liquid, possessing molar mass of 221.37 g mol^{-1}, density of 0.946 g cm^{-3} and melting point of 217 °C. It is highly moisture sensitive and slightly toxic. APTES was obtained from Sigma Aldrich, USA and used as received.

Toluene (PhMe) was used as a solvent for preparation of Si-GO. It is a colorless liquid, having molar mass of 92.14 g mol^{-1}, density of 0.867 g cm^{-3} and boiling point of 110 °C. PhMe was purchased from Merck, India and dried to remove water content, prior to use.

Chloroform ($CHCl_3$) was used as a solvent for preparation of Si-GO. It is a colorless liquid, having molar mass of 119.37 g mol^{-1}, density of 1.489 g cm^{-3} and boiling point of 61 °C. $CHCl_3$ was purchased from Merck, India and dried to remove water content, prior to use.

4.2.2. Methods

4.2.2.1. Preparation of Si-GO

Graphene oxide (GO) was prepared initially from graphite flakes by a modified Hummers' method [13], as described in Chapter 3 (Section 3.2.2.1). Si-GO was prepared by the chemical functionalization of GO using APTES, as per modification of an earlier reported procedure [14, 15]. In a typical process, a stable dispersion of 1 g GO in 50 mL of dry PhMe

was achieved by overnight mechanical stirring, followed by ultrasonication. A solution of 5 mmol (1.105 g) of APTES in 20 mL of dry $CHCl_3$ was added to the GO dispersion. The mixture was stirred at 100 °C in a pre-heated oil bath for 5 h under N_2 atm to obtain the desired Si-GO. The resultant dispersion was filtered and washed with dry $CHCl_3$ (5 x 20 mL) to remove the unreacted APTES. The purified Si-GO was re-dispersed in dry $CHCl_3$ (25 mL) and stored at 25 °C. A small amount of the material was vacuum oven dried at 40 °C for structural analysis.

4.2.2.2. Fabrication of HPU/Si-GO nanocomposite

Fabrication of HPU/Si-GO nanocomposite was achieved by an *in situ* polymerization technique, following the same process as described in Chapter 3 (Section 3.2.2.1). Only in this case, a stable dispersion of Si-GO (in dry THF) was incorporated in the second step of the polymerization reaction under constant mechanical agitation.

HPUNC with different weight percentages of Si-GO, *viz.* 0.5 wt%, 1.0 wt% and 2.0 wt% were prepared and encoded as HPU/Si-GO0.5, HPU/Si-GO1.0 and HPU/Si-GO2.0 respectively. In the same way, pristine HPU was prepared without using Si-GO for comparison purpose. Pristine HPU is equivalent to HPU3, as described in Chapter 2 and used as the matrix.

4.2.2.3. Sample preparation for performance study

Samples of HPUNC compositions were prepared by the same process as HPU, as described in Chapter 2 (Section 2.2.2.3). All analysis and testing were performed using bulk HPUNC samples without any further purification.

4.2.2.4. Self healing study

The self healing behavior of HPU/Si-GO nanocomposites was studied by mechanically damaging the polymer film strips in transverse direction by a razor blade (approximate cut of 5 mm length and 0.2 μm depth) and then healing them by using different stimuli like microwave and sunlight. Microwave healing was performed using a domestic microwave oven operating at 2.45 GHz frequency and 450 W power output. Sunlight healing was achieved under direct sunlight (11 am-2 pm) at Tezpur University campus (altitude: 26.63 °N 92.8 °E) in the month of October at sunny days [average temperature (30±1 °C) and humidity (60±1 %), light intensity: 10^6 lux]. The optimal healing time was considered as the shortest time required for achieving best healing under the applied conditions. The healing efficiency (%) was calculated by measuring the percentage ratio of tensile strength of the films before damage and after healing of damage.

4.2.2.5. Surface hydrophobicity study

The surface hydrophobicity of the nanocomposite films was evaluated by contact angle measurements. Samples of 2 cm × 2 cm dimensions were first dried at 40 °C in a hot air oven for 2 h and then stick to a glass slide for analysis. The static contact angles values were measured by using Millipore water at three different locations on the polymer film surface after the drops were allowed to settle and equilibrate with the environment.

4.2.2.6. Surface free energy measurement

The surface free energy (SFE) measurements were done on the basis of the Owens-Wendt method. [16, 17] The Owens-Wendt model assumes that the surface free energy $\gamma_{S,L}$ may be presented as a sum of two components:

$$\gamma_{S,L} = \gamma^{d}_{S,L} + \gamma^{p}_{S,L} \quad \textbf{(Eq. 4.1)}$$

where, $\gamma^{d}_{S,L}$ is the surface energy connected with dispersion interactions and $\gamma^{p}_{S,L}$ is surface energy connected with polar acid–base interactions. The equation is valid for a solid phase (S) as well as wetting liquid (standard liquid or tested liquid, L).

The SFE value for solids (S) and for liquids (L) which interact with those solids should satisfy the Owens–Wendt equation:

$$\gamma_L \times \frac{1+\cos\theta}{2} = \sqrt{\gamma^{d}_{S}} \times \sqrt{\gamma^{d}_{L}} + \sqrt{\gamma^{p}_{S}} \times \sqrt{\gamma^{p}_{L}} \quad \textbf{(Eq. 4.2)}$$

where, θ is the experimentally found static contact angle between the liquid drop and the solid surface under investigation. The values of θ were first evaluated for the surfaces of HPU and its nanocomposite films with the use of a pairs of model liquids (water–diiodomethane) with known parameters. Then, **Eq. 4.2** was used to calculate the values γ^{d}_{S} and γ^{p}_{S} for the studied polymer films. The values of γ_S were calculated from **Eq. 4.1.**

4.2.3. Characterization

FT-IR, UV-Vis, XRD, SEM, TGA and DSC analyses of the nanohybrid and HPUNC were performed by the same instruments and under same conditions, as mentioned in Chapter 2 (Section 2.2.3). Raman, TEM and EDX analyses of the nanohybrid and nanocomposite were executed by the same instruments with same specifications, as described in Chapter 3 (Section 3.2.3). Various mechanical testing of the HPUNC films *viz.* tensile strength, elongation at break, scratch hardness, impact resistance, etc. were performed by the same instruments and under the same conditions as described in Chapter 2 (Section 2.2.3). Chemical resistance testing of the HPUNC films was performed under the same conditions, as described in Chapter 2 (Section 2.2.3).

The static water contact angles on the nanocomposite films were measured by using a contact angle instrument (Model: DSA 25, Kruss, Germany). The self healing behavior of the nanocomposite films were visualized by using a polarizing optical microscope (Model: BA310Pol, Motic, USA) at 10x magnification with 0.25 D power.

4.3. Results and discussion

4.3.1. Preparation and characterization of Si-GO

Si-GO was prepared by chemical modification of GO with APTES as depicted in **Scheme 4.1.**

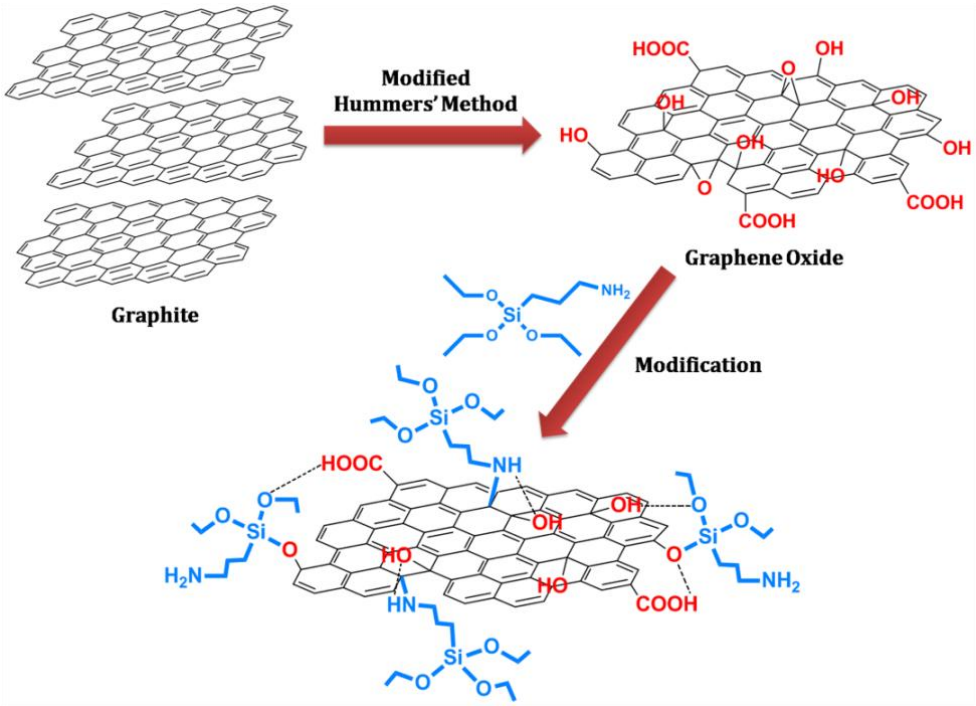

Scheme 4.1. Preparation of Si-GO.

Initially, a proper dispersion of GO in xylene was attained from exfoliation of stacked GO sheets. GO sheets contain hydroxyl and epoxy groups on its basal plane, along with the carboxylic groups on the edges [13]. In this study, these oxygeneous functional groups facilitated the chemical interaction between APTES and the GO sheets. APTES presumably underwent ring opening of epoxy groups of GO with the amine functionality and nucleophilic substitution of the labile ethoxy groups with the hydroxyl and carboxyl moieties of GO, thereby covalently linking with GO sheets, in addition to some secondary interactions [14, 18].

FT-IR spectroscopy offered a credible insight into the modification of GO with APTES, as shown in **Figure 4.1.a.**

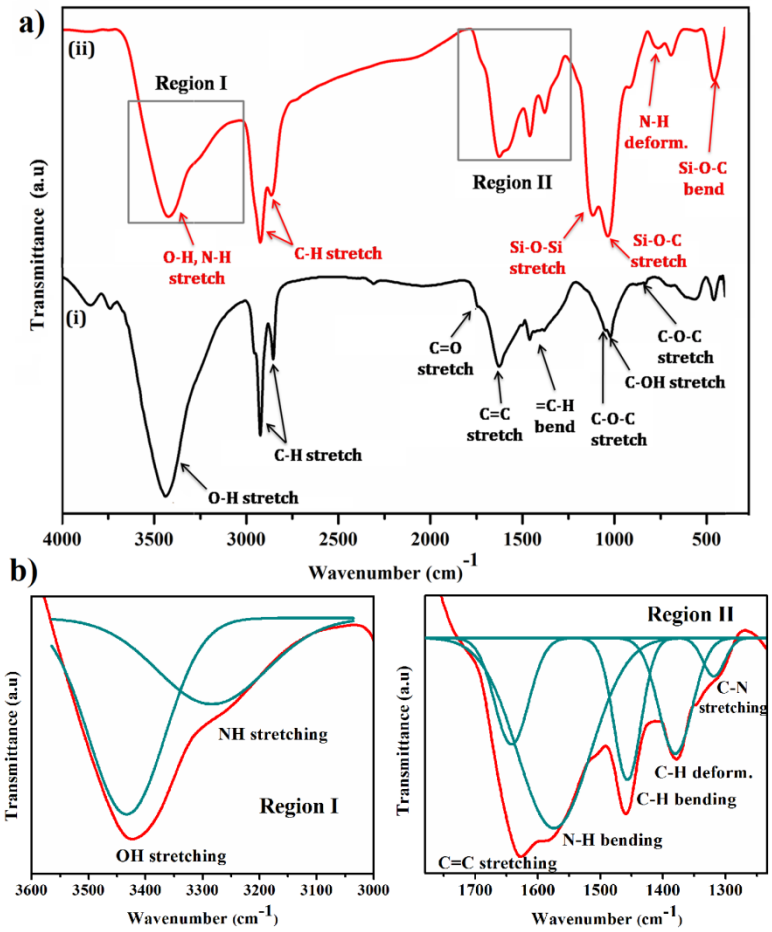

Figure 4.1. a) FT-IR spectra of i) GO and ii) Si-GO, and **b)** Deconvoluted region I and II of FT-IR spectrum of Si-GO.

GO demonstrated its characteristic vibrational bands at 1740 cm^{-1} (C=O stretching of carboxylic groups), 1627 cm^{-1} (C=C stretching of graphitic framework) and 1020 cm^{-1} (C-OH stretching of alkoxyl and phenolic groups) in the spectrum [13]. The C-O-C/C-O vibrations of epoxide groups in GO appeared at 1052 cm^{-1} and 830 cm^{-1}. The C-H vibrational bands of the graphitic structure in GO emerged at 2923 cm^{-1} (asymmetric stretching), 2853 cm^{-1} (symmetric stretching) and 1459 cm^{-1} (bending) respectively. The sharp peak at 3440 cm^{-1} can be assigned to O-H stretching of hydroxyl groups and absorbed water molecules in GO. In contrast to GO, Si-GO displayed noticeable variations and emergence of new bands. These variations included, a broad band centered at 3420 cm^{-1} possibly due to overlapping of O-H and N-H stretching vibrations, which was clearly visible after deconvolution of the region (Region I of **Figure 4.1.b**). The C-H stretching bands were sharpened and the carboxylic C=O stretching band diminished at 1729 cm^{-1}. Deconvolution of region between 1800-1300 cm^{-1} revealed multitude of bands (Region II of **Figure 4.1.b**) featuring C=C stretching band at 1628 cm^{-1} and secondary N-H bending band at 1586 cm^{-1} that converged together. Medium intensity bands of C-H bending and deformation

appeared at 1459 cm^{-1} and 1377 cm^{-1}. A weakened C-N stretching band emerged at 1309 cm^{-1}, along with N-H deformation band at 765 cm^{-1}. The sharp new bands at 1117 cm^{-1} (Si-O-Si stretching), 1035 cm^{-1} (Si-O-C stretching) and 459 cm^{-1} (Si-O-C bending) provided supportive evidence for functionalization of GO by APTES [14, 15, 18, 19].

Raman spectral analysis also provided ample evidence in support of modification of GO sheets. It is well known that graphitic materials display two fundamental bands *viz.* D band and G band. The D band arises due to structural defects in the graphitic domains, while G band arises due to the in-plane stretching of the sp^2 hybrid carbons atoms [13]. The Raman spectra of GO and Si-GO, as shown in **Figure 4.2.a**, displayed two fundamental bands, D band and G band, for both GO and Si-GO at 1370 cm^{-1} and 1615 cm^{-1} respectively. In this study, the intensity ratio of D band to G band (I_D/I_G) showed a miniature change from 0.95 to 0.97 after modification of GO to Si-GO. These observations can be attributed to the insertion of the APTES moiety in GO sheets. The presence of APTES contributed to the structure defects in GO, suggesting creation of new graphitic domains, leading to slight increase in I_D/I_G ratio [19]. XRD results presented another conclusive support in favor of functionalization of GO, as demonstrated in **Figure 4.2.b**. XRD patterns of GO showed an intense peak at $2\theta = 9.85°$, attributed to (002) plane of oxidized graphitic domains, with *d*-spacing of 8.97 Å, which is larger than that of graphite (3.4 Å) [20]. This can be mainly attributed to the presence of oxygeneous functionalities and trapping of water molecules in the interspaces of GO sheets [21]. However, on modification with APTES, the peak shifted to $2\theta = 11.69°$, corresponding to *d*-spacing of 7.56 Å. This slight decrease in interlayer distance can be assigned to insertion of APTES between layers and escape of water molecules. The insertion of APTES in GO, probably released some of the absorbed water molecules on interaction with oxygeneous groups and strengthened the physical interactions of the layers, ultimately decreasing the interlayer distance. Interestingly, the appearance of another broad peak near $2\theta = 21.21°$ was observed in Si-GO, typical of amorphous SiO_2 [22], which may be due to formation a small amount of silica particles by interaction of APTES moiety with absorbed water molecules. It is to be noted that GO samples contains numerous oxygen functionalities that absorb water from air at ambient humidity and complete drying of samples seems to be very difficult. Therefore, the values of *d*-spacing mentioned herein might reflect different abilities of samples to become hydrated by air at ambient humidity [23]. EDX elemental analysis of Si-GO, presented in **Figure 4.2.c**, confirmed the presence of elements *viz.* carbon, oxygen, nitrogen and silicon, with corresponding wt% of 48.25, 29.94, 12.48 and 9.33, as expected from the modification of GO. TG analysis of GO and Si-GO, as depicted in **Figure 4.2.d,** demonstrated distinct

variation in their degradation patterns, which can be viewed as evidence of chemical functionalization of GO.

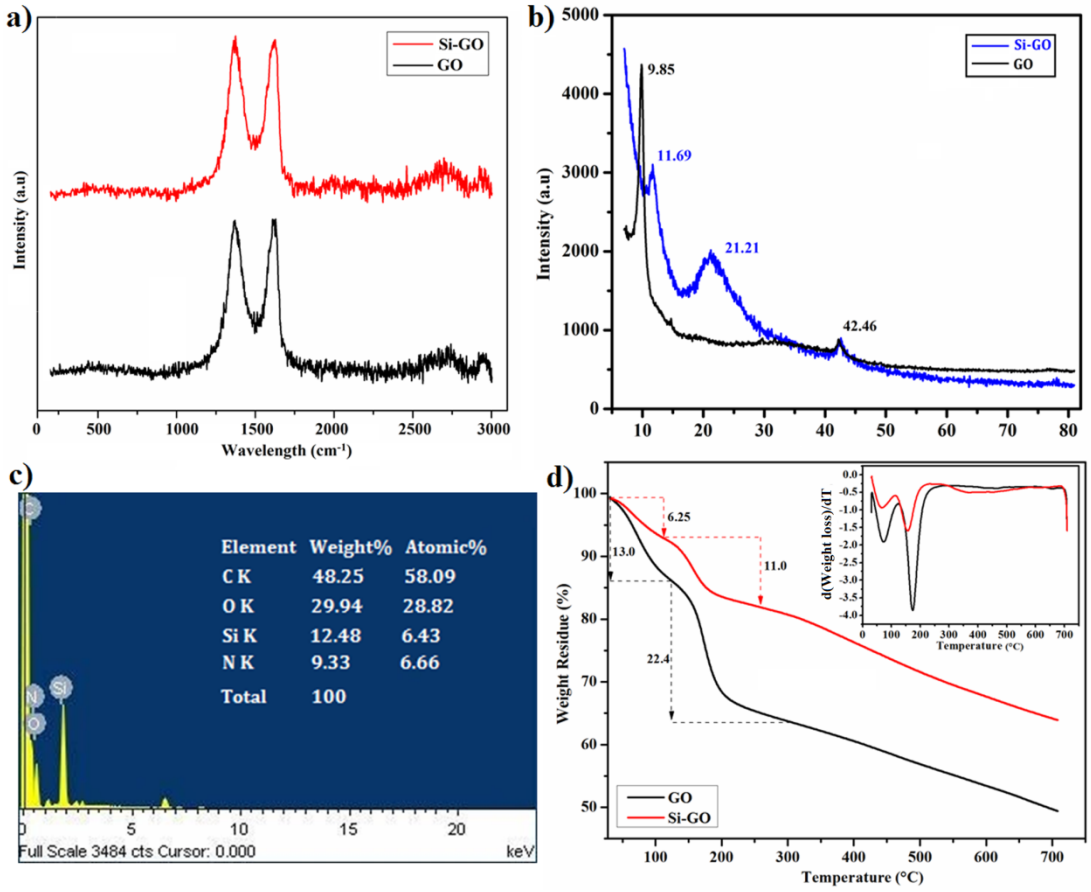

Figure 4.2. a) Raman spectra of GO and Si-GO, **b)** XRD patterns of GO and Si-GO, **c)** EDX map of Si-GO, and **d)** TG thermograms of GO and Si-GO (inset: dTG curves of GO and Si-GO).

As mentioned earlier, GO contains numerous oxygeneous functionalities in their graphitic domains and can easily absorb water from air. In this study, GO showed 13.0% weight loss near 100 °C, due to evaporation of absorbed water molecules by these oxygeneous functionalities between the interspaces [20]. This was followed by a sharp weight loss of 22.4% in the range of 120-300 °C, owing to the removal of the oxygeneous functionalities and thereafter weight loss beyond 400 °C due to pyrolysis of graphitic domains of GO [18, 21]. In stark contrast, Si-GO displayed 6.25% weight loss around 100 °C attributed to the removal of absorbed water molecules, followed by 11% weight loss in the range of 110-260 °C, possibly due to the removal of free oxygeneous moieties unbounded to APTES. Compared to the TG curve of GO, weight loss of Si-GO in the range of 120-300 °C and below 300 °C was much lower, suggesting the anchoring of APTES moiety to the oxygeneous groups of GO. The significant weight loss beyond 300 °C seen for Si-GO probably implied the degradation of APTES moieties and graphitic skeleton [15, 18].

Overall, it was observed that Si-GO displayed much lesser thermal degradation than GO, which can be attributed to presence of APTES-bound GO sheets.

4.3.2. Fabrication and characterization of HPU/Si-GO nanocomposite

HPU/Si-GO nanocomposites were fabricated by an *in situ* polymerization technique, where castor oil modified polyol was employed as the branch generating unit and Si-GO as the nano-filler, as shown in **Scheme 4.2.**

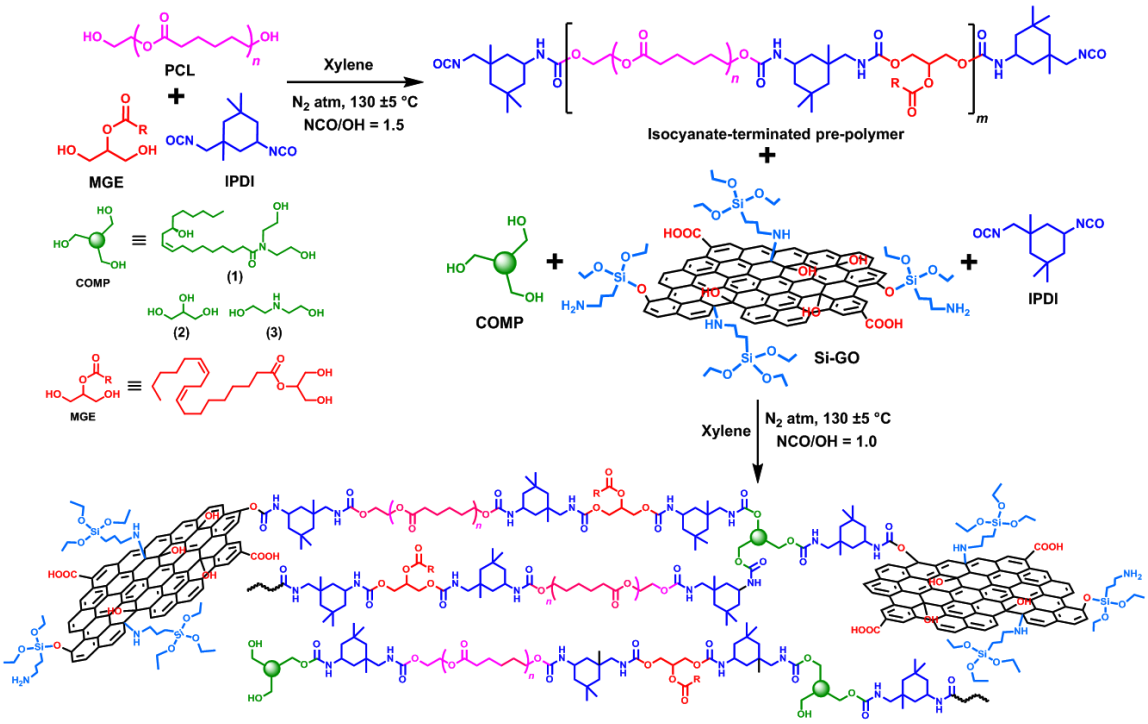

Scheme 4.2. Fabrication of HPU/Si-GO nanocomposite.

Dispersibility of the nanomaterial in the polymer matrix is a crucial criterion for the formation of nanocomposite, as it significantly influences its performance. In this context, the HPU matrix was found to be suitable for the formation of nanocomposite. The presence of large number of polar moieties in its molecular chain plays a pivotal role in integrating the nanomaterial in the matrix [24]. To ensure the formation of a uniformly distributed nanocomposite, a stable dispersion of the nanomaterial was incorporated in the second step along with the branch generating unit. This strategy provided a better route for assimilating the nanomaterial in the HPU matrix *via* strong interfacial interactions with the multi-functional moiety and the pre-polymer. Another important criterion to be considered during polymerization is the concentration of the multi-functional moiety. The multi-functional moiety was administered dropwise as a very dilute solution (15% in xylene) in the second step and maintained at 60% dilution (in xylene) throughout to prevent gel formation till the end of the reaction [25].

FT-IR analysis of the nanocomposites gave insight into the chemical composition of the HPU matrix. The presence of key functional bands such as N-H stretching (of urethane linkage) at 3440 cm^{-1}, C-H stretching at 2926 cm^{-1} and 2853 cm^{-1}, C=O stretching (of ester) at 1750 cm^{-1}, C=O stretching (of amide) at 1631 cm^{-1}, C-H bending at 1460 cm^{-1}, C-N & C-O stretching at 1130 cm^{-1}, C-O-C stretching at 1048 cm^{-1} and N-H deformation at 669 cm^{-1}, as seen in **Figure 4.3** confirms the presence of urethane bonding in the nanocomposite [25, 26]. Also, it is worth noting that there were no significant bands observed for Si-GO in the spectra. This might be due to a very small amount of the nanomaterial dispersed in the polymer (upto 2 wt% with respect to HPU), which was overwhelmed by other functional groups of the polymer. Surface morphological studies of HPU/Si-GO nanocomposite displayed clear distinction from that of pristine HPU. SEM images of pristine HPU revealed smooth texture of the polymer matrix, devoid of any perturbation, as seen in **Figure 4.4.a**. On the contrary, the SEM images of the nanocomposites displayed micro-roughness and uneven textures, as observed in **Figure 4.4.b**. This observation suggested formation of strong interfacial interactions between the polymer matrix and the nanomaterial. The intercalation of the nanomaterial in between the polymeric chains of HPU created perturbations due to their structural incompatibility, resulting in rough texture of the matrix [27]. Bulk morphology studies of the HPU/Si-GO nanocomposite by TEM revealed the uniform dispersion of Si-GO sheets in the polymer matrix, seen in **Figure 4.4.c**. TEM images of HPU/Si-GO in **Figure 4.4.d** displayed textured morphology of the chemically modified Si-GO sheets, embedded in the polymer matrix.

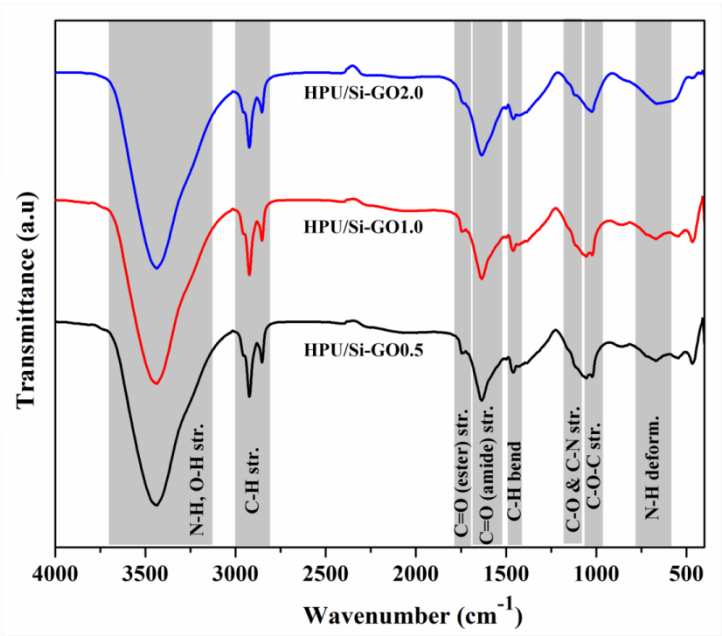

Figure 4.3. FT-IR spectra of HPU/Si-GO nanocomposites.

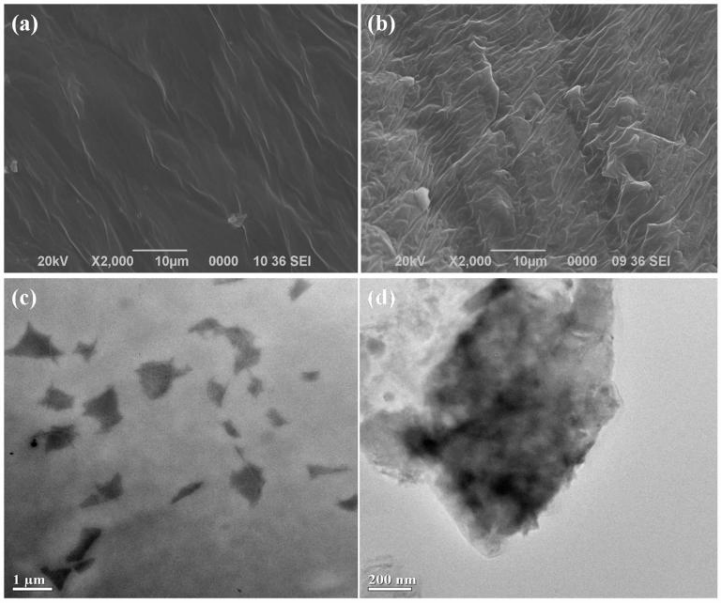

Figure 4.4. SEM images of fractured surface of **a)** pristine HPU and, **b)** HPU/Si-GO0.5, and TEM images of HPU/Si-GO0.5 at magnification of **c)** 1 μm and, **d)** 200 nm.

4.3.3. Mechanical properties

The HPU/Si-GO nanocomposites exhibited excellent mechanical properties like tensile strength (σ), elongation at break (ε), toughness (T), scratch hardness and impact strength, as shown in **Table 4.1**. The incorporation of Si-GO nanosheets reinforced the HPU matrix and imparted high mechanical performance in terms of the aforementioned properties. Especially, HPU/Si-GO nanocomposites showed huge improvement in values of σ, ε, and T, in comparison to pristine HPU at very low Si-GO loading (upto 2 wt%), as evident from stress-strain curves, shown in **Figure 4.5**. Further, the mechanical properties showed dependency on loading of the nanomaterial.

Table 4.1. Mechanical properties of HPU and its nanocomposites

Property	HPU	HPU/ Si-GO0.5	HPU/ Si-GO1.0	HPU/ Si-GO2.0
Tensile strength, σ (MPa)	5.2 ± 0.1	7.5 ± 0.1	12.7 ± 0.2	10.0 ± 0.5
Elongation at break, ε (%)	607 ± 3	906 ± 4	1011 ± 5	1248 ± 2
Toughness[a], T (MJm^{-3})	27.8 ± 0.5	36.4 ± 0.1	75.46 ± 0.2	94.6 ± 0.5
Scratch hardness[b] (kg)	10	>10	>10	>10
Impact strength[c] (kJm^{-1})	19 ± 0.2	18.6 ± 0.2	19.2 ± 0.1	19.0 ± 0.1

[a]Calculated by integrating the stress-strain curves. [b]Maximum limit is 10 kg. [c]Converted to energy unit per thickness of sample (thickness of sample between 0.40 mm – 0.45 mm).

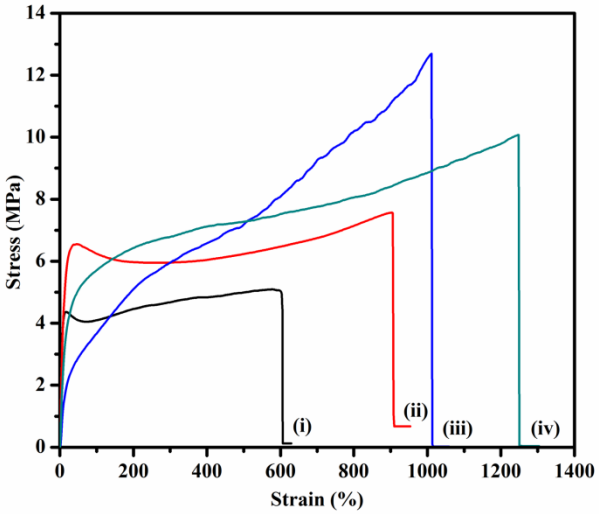

Figure 4.5. Stress-strain profiles of (i) HPU and (ii)-(iv) HPU/Si-GO nanocomposites.

Values of σ showed an uneven trend with respect to content of nanomaterial. Initial loading of 0.5 wt% showed 144% increase in σ, followed by 247% increase at 1 wt% loading. Proper dispersion of Si-GO and strong interfacial interactions through covalent/non-covalent bonding between HPU matrix and Si-GO resulted in reinforcement and chain stiffening of the hard segments, thereby increasing the rigidity of the matrix. In addition, multiple secondary interactions like H-bonding, van der Waals' interactions, $\pi-\pi$ stacking interactions between Si-GO and HPU matrix enhanced the structural compactness and rigidity. This resulted in effective load transfer between HPU matrix and nanomaterial, thereby resulting in high σ values [28, 29]. Further, increase in nanomaterial content to 2 wt% resulted in reduction of σ to ~196%. This reduction in σ can be assigned to a high yield stress which altered the orientation of the hard segments, along with improper reinforcement of HPU matrix due to possible agglomeration of Si-GO in the matrix. Higher content of the nanomaterial in the HPU matrix may have hindered secondary interactions with polymer chains, because of their stronger affinity for $\pi-\pi$ stacking interactions and lowered the rigidity of the matrix [30]. At the same time, values of ε were found to be increased upto ~206% following an increasing trend with the increasing content of nanomaterial. Initial loading of 0.5 wt% Si-GO recorded a 149% increase in ε, followed by 167% increase in ε at 1.0 wt% loading and ultimately a very high enhancement of 206% at 2.0 wt%. This significant and unusual enhancement of ε can be ascribed to the high flexibility and mobility of soft segments in combination with the Si-GO-reinforced polymeric chains. The increasing nanomaterial content in the polymer matrix imparted a steady rising of ε by extension of coiled polymer chains along the elongating direction and sliding of the some agglomerated Si-GO layers passed one another by lengthening its $\pi-\pi$ stacking interactions [27, 31]. Additionally, secondary "sacrificial" interactions between the

coiled polymer chains and Si-GO also contributed to this enhancement of ε. These sacrificial bonds ruptured under the applied stress instead of primary covalent bonds, allowing further elongation of the coiled polymer chains [31]. In addition, the nanocomposites also recorded a sequential enhancement in toughness upto ~339%, with increasing nanomaterial loading upto 2 wt%. Since toughness of the material is a combination of its rigidity and flexibility, hence the synergistic effect of stiffness and mobility of the Si-GO reinforced polymer segments and multiple secondary interactions therewith contributed to this result [27, 31]. This synergistic effect allowed smooth dissipation of applied load by elongation of the reinforced polymer segments, at the same time maintaining their structural integrity through its chain stiffness. In the same vein, all the nanocomposites displayed high scratch hardness, due to increase in toughness of the material. Similarly, the toughness and the net strength of the polymeric material contributed to high impact strength of the nanocomposites. In fact, both scratch hardness and impact strength recorded was found to be more than the limit of the instrument in all the cases, however in the case of impact strength, conversion to energy unit per thickness of the polymer films, comparable values were obtained.

4.3.4. Thermal properties

TG analysis of HPU/Si-GO nanocomposites demonstrated excellent stability towards thermal degradation. The TG and dTG curves in **Figure 4.6.a** and **4.6.b** reveal very high thermal threshold above 300 °C for the nanocomposites, much more than that of pristine HPU. Pristine HPU with its purely aliphatic matrix showed less resistance to thermal degradation than that of the nanocomposites. This enhanced thermal stability of nanocomposites can be accredited to the presence of APTES-bound GO nano-sheets dispersed in the HPU matrix, making the system more compact *via* strong covalent and non covalent interactions with the polymer chains. These nano-sheets reinforced the polymer matrix by occupying the voids, leading to restriction in thermal motion of the polymer chains, thereby increasing thermal stability [29, 32]. Also, the presence of APTES moiety provided a thermally insulating effect on the polymer matrix [19]. The presence of Si-GO balanced the energy dissipation to the matrix by absorbing the energy and hindered the pyrolysis of the reinforced polymer segments, enhancing the thermal stability [33, 34]. Further, all the nanocomposites showed enhancement of thermal degradation temperatures, corresponding to the increase in nanomaterial loading.

DSC curves shown in Figure **4.6.c** revealed no variation in the glass transition temperature of the soft segments (T_g) of HPU and their nanocomposites. On the other hand, the hard segments ($T_{g'}$) of HPU and their nanocomposites displayed an increasing trend

with the incorporation of Si-GO content This suggested the preferential reinforcement of the hard segments of the HPU matrix by the nanomaterial [29, 31]. In a similar vein, the melting transition temperature (T_m) of soft segments of HPU and their nanocomposites showed a rising trend with increasing Si-GO content. This observation reiterated the nucleating and reinforcing ability of graphene nano-sheets, restricting the thermal mobility of the polymer chains [33, 34]. Such temperature increment with increasing nanomaterial loading was also supported by TG analysis.

4.3.5. Chemical resistance study

The chemical resistance of HPU/Si-GO nanocomposites was tested in different chemical media *viz*. 10% aqueous NaCl (w/v), 20% aqueous ethanol (v/v), 5% aqueous HCl (v/v), 3% NaOH (w/v) and normal tap water as displayed in **Figure 4.6.d**.

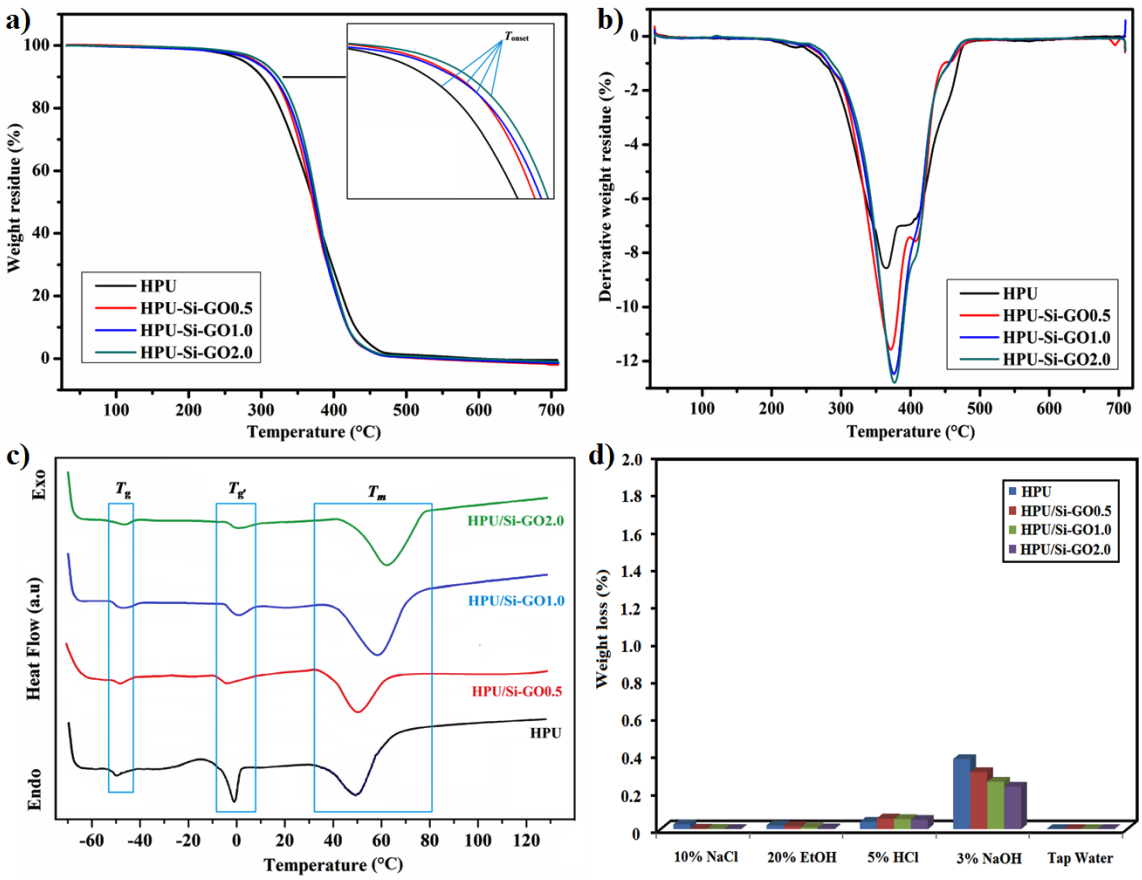

Figure 4.6. a) TG thermograms, **b)** dTG curves, **c)** DSC curves and**, d)** Chemical resistance in different chemical media, of HPU and HPU/Si-GO nanocomposites.

All the nanocomposites showed high chemical resistance in the tested chemical environments with weight loss of less than 0.1%, except in alkali medium. This exhibition of good chemical resistance can be attributed to the robust nanocomposite system by the

means of hyperbranched structure and various secondary interactions like hydrogen bonding, polar-polar interactions, van der Waals interactions in the HPU matrix [25]. However, the comparatively higher weight loss in alkali medium reflected the presence of hydrolysable ester linkages in the polymer matrix.

4.3.6. Self healing study

The self healing ability of the nanocomposites was examined from optical images and by tensile strength test, wherein mechanical damage inflicted on the film was healed by different stimuli like microwave and sunlight. Optical images displaying self healing behaviors of HPU and HPU/Si-GO nanocomposite films on exposure to sunlight are shown in **Figure 4.7**.

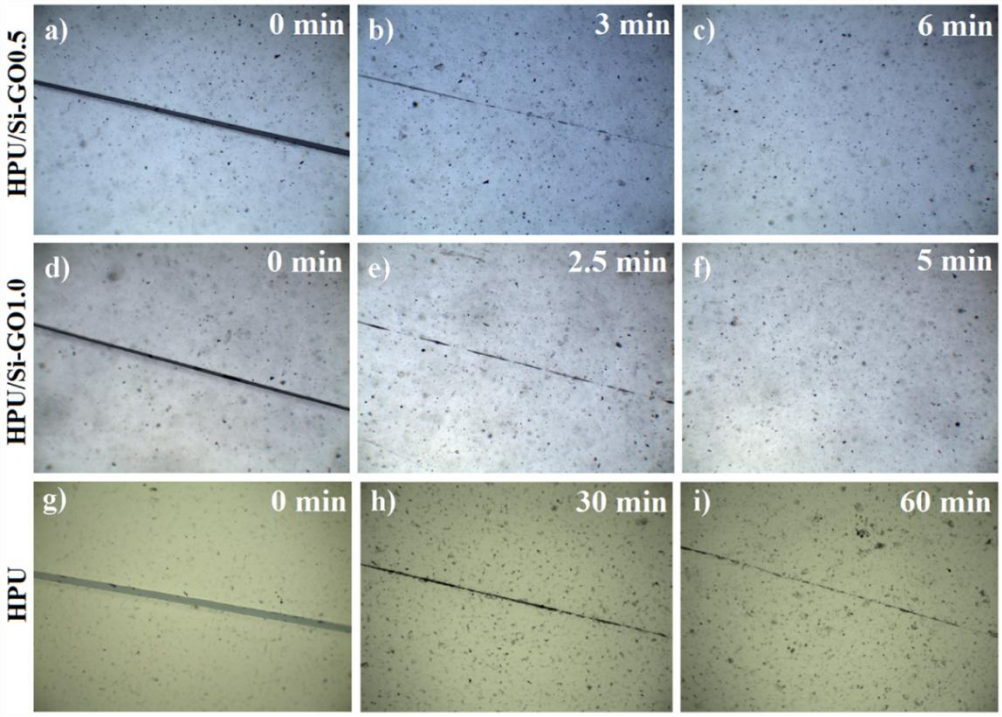

Figure 4.7. Optical images displaying self healing behaviors of HPU/Si-GO0.5, HPU/Si-GO1.0 and HPU under exposure to direct sunlight.

It is well known that PU is composed of innate combination of hard and soft segments [2]. Both of these segments contribute to the self healing process through supramolecular self assembly, involving diffusion and subsequent rearrangement/ recombination of polymeric segments in the damaged area [2]. The soft segment of PU undergoes rapid Brownian motion on switching of its glass transition temperature or melting temperature and lead to the diffusion and rearrangement of molecular chains in the damaged area. Meanwhile, the hard segments provide the structural rigidity and

maintain the original shape of the material intact [8, 9]. This self healing ability is assisted by shape memory effect (SME) of PU that brings the polymeric chains in close proximity at the damaged area.

In this study, the nanocomposites displayed good self healing ability by MW and sunlight. This self healing ability of the HPU/Si-GO nanocomposites can be credited to the alteration in segmental distribution of the HPU matrix by action of applied external stimulus. This applied external stimulus resulted in excitation of some polar moieties in the vicinity of the damaged area. This excitation energy switched the melting transition temperature of the soft segments near the damaged area of the HPU matrix, causing diffusion of the soft segments and subsequent rearrangement of molecular polymeric chains to heal the damaged surface. This healing process was augmented by the presence of Si-GO nano-sheets in the polymer matrix. The graphitic domains of Si-GO acted as nanoheater, absorbing energy from the external stimulus and dissipating the energy to the polymer matrix, which in turn drove the self healing process [29]. External stimuli like microwave (MW) and sunlight were found to be suitable for this purpose. However, MW healing was found to be more expeditious than sunlight healing. Both MW and sunlight were sufficient to trigger the self healing tendency of the polymer matrix by effective heating of the HPU matrix. The surface temperature of the nanocomposites was found to be 50 (± 5) °C, which was near to the melting transition temperature of the soft segments of HPU matrix. The probable self healing mechanism of the nanocomposite was illustrated in **Figure 4.8.a**. However, in contrast to the nanocomposites, the pristine HPU did not show complete healing of the damaged film upon exposure to different stimuli even after a long time (**Figure 4.7.g-i**). This indicated the insufficiency of polymer matrix to achieve self healing on its own by absorbing the required energy from the external stimulus. In this perspective, it is pertinent to mention that pristine HPU show a shape memory effect (SME) but not self healing ability, even though both of these processes involve rearrangement of polymeric chains. This is because energy requirement for activation of the polymeric chains for rearranging its orientation and gaining its original shape is less compared to diffusion of the polymeric chains in the damaged area. A huge amount of energy is required to melt a particular segment of polymer and permit chain diffusion process [24]. Pristine HPU contains few polar groups that can absorb energy from stimulus, which is sufficient only for SME and not for polymeric chain diffusion. Hence, HPU showed incomplete self healing ability by virtue of SME. However, the presence of Si-GO was instrumental in bringing about effective healing of the nanocomposites. This can be attributed to Si-GO acting as a nanoheater in the polymer matrix that provided the extra impetus for complete self healing. The nanocomposites showed enhancement of self healing behavior with increase

in nanomaterial content. This enhancement can be attributed to more amount of nanomaterial embedded in the polymer matrix, thereby increasing the energy mobilization required for healing process. Repetition of healing is an important criterion for self healing materials, as it manifest in longevity of the material. In this work, self healing was accomplished by rearrangement of soft segments of HPU, with the aid of SME and heating ability of Si-GO nano sheets. As a result, repeated healing of the nanocomposite films was achieved. The healing efficiencies of nanocomposites were evaluated by tensile strength measurements of the films upon exposure to MW and sunlight as shown in **Figure 4.8.b**. The healing ability of films remained almost same upto fourth cycle of healing upon exposure to both MW and sunlight. Stress-strain profiles of the nanocomposite in **Figure 4.8.c** demonstrated comparable tensile strength values recorded before and after healing.

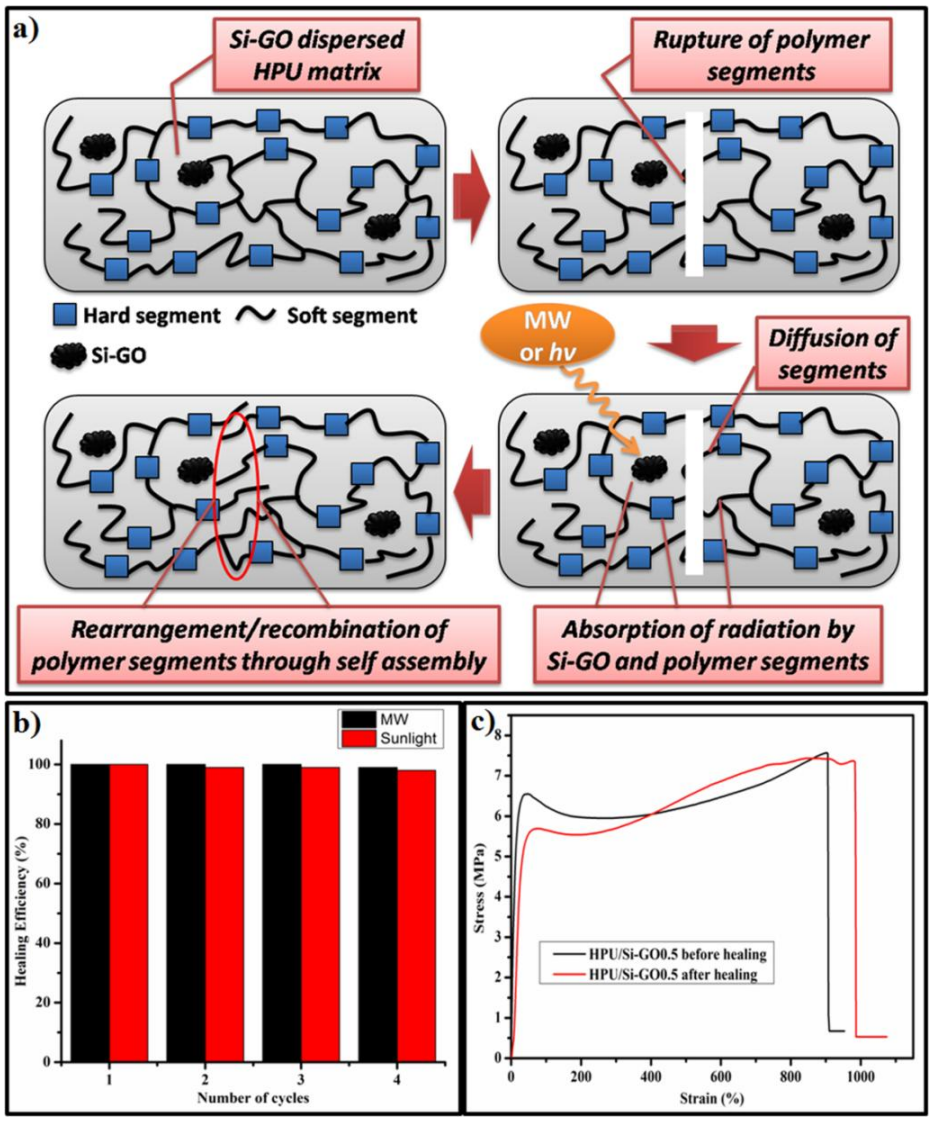

Figure 4.8. a) Self healing mechanism of HPU/Si-GO nanocomposites, **b)** Healing efficiencies of HPU/Si-GO0.5 nanocomposite under MW and sunlight, and **c)** Stress-strain profiles of HPU/Si-GO0.5 before and after healing.

4.3.7. Surface hydrophobicity study

The surface hydrophobicity of the HPU and its nanocomposites was studied with static water contact angle measurements on the surface of the films and the results stated in **Table 4.2**. Surface hydrophobicity of a material depends upon two significant factors: low surface energy of the material and surface geometrical structures or roughness [5]. The high water contact angles made on the surface are indicative of low surface energy which inhibits the adhesion of the free surface bonds with water molecules by various physico-chemical interactions and surface roughness. These do not allow the water molecules to soak into the surface. Both of these factors combine to prevent the complete wetting of the surface [35, 36].

In this study, the chemical composition of the nanocomposites, primarily the HPU matrix provided the intrinsic hydrophobic character. The HPU matrix contained non polar, purely aliphatic long hydrocarbon chains [25], which imparted low surface energy to the nanocomposites. The surface energy of the HPU and its nanocomposites was evaluated on basis of Owens-Wendt model as shown in **Table 4.3**. The surface energy of HPU was found to be 49.18 mJ/m^2, while the surface energy of the nanocomposites was in the range of 53-58 mJ/m^2. The surface energy of the nanocomposites was found to be less than that of pristine HPU, which can be attributed to contributions from Si-GO with its graphitic domains and silane moiety. At the same time, the presence of the Si-GO nano-sheets in the HPU matrix resulted in development of surface micro-roughness, due to the structural incompatibility of the purely aliphatic organic polymer matrix and graphitic domains and inorganic constituent of Si-GO. This observation was supported by SEM results, as discussed earlier. The surface hydrophobicity of the nanocomposites displayed an increasing trend through static water contact angles, with the increase in the nanomaterial loading as shown in **Figure 4.9.b-d**. This can be attributed to increase in surface roughness, due to incorporation of more amount of nanomaterial in the polymer matrix. 3D surface area plot in **Figure 4.9.e,** derived from the optical image of HPU/Si-GO1.0 revealed the existence of surface micro-roughness. The film strips of the nanocomposites demonstrated self cleaning ability *via.* surface hydrophobicity as shown in **Figure 4.9.f-h**, where the dirt-covered surface of HPU/Si-GO1.0 was cleaned by small water droplets without complete wetting of the surface. The pristine HPU was devoid of hydrophobic character, showing very low water contact angles (< 90°) (**Figure 4.9.a**). This can be attributed to the smooth surface of polymer matrix, as seen earlier in SEM results, despite the presence of non polar aliphatic chain moieties. This reiterated the fact that only low surface energy is insufficient in inducing high hydrophobicity, and surface roughness is a significant criterion.

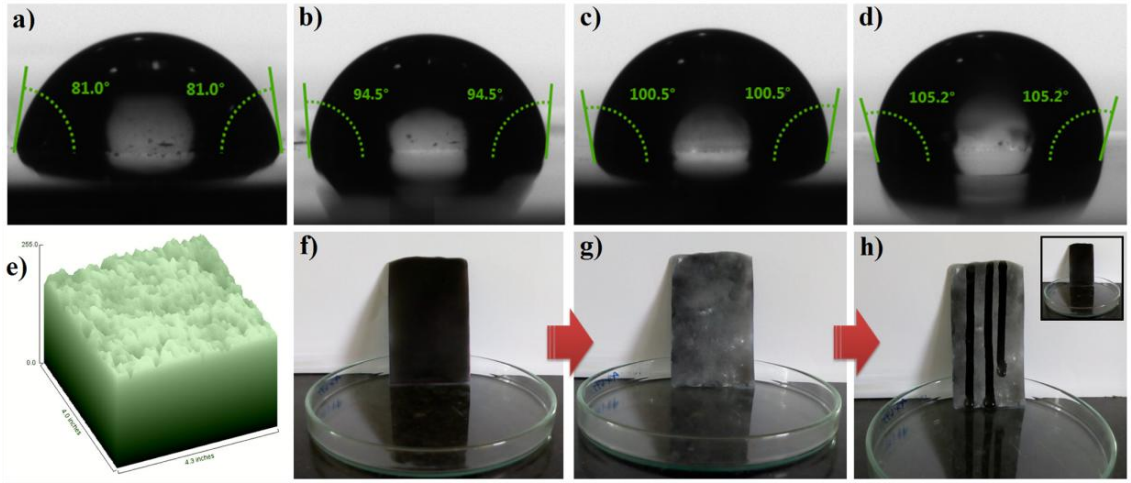

Figure 4.9. a)–d) Optical images displaying static water contact angles of HPU, HPU/Si-GO0.5, HPU/Si-GO1.0 and HPU/Si-GO2.0 respectively, **e)** 3D surface plot of HPU/Si-GO1.0, and **f)–h)** Self cleaning ability of dirt-covered HPU/Si-GO1.0 film with water droplets (inset HPU/Si-GO1.0 film after cleaning).

Table 4.2. Surface properties and static contact angles of model measuring liquids

Model liquid	Surface free energy parameters			Contact angle (°)			
	γ_L	$\gamma^d{}_L$	$\gamma^p{}_L$	HPU	HPU/ Si-GO0.5	HPU/ Si-GO1.0	HPU/ Si-GO2.0
Water	72.8	21.8	51	81	94.5	100.5	105.2
Diiodomethane	50.8	48.5	2.3	10	8	5	4
Calculated surface energy mJ/m^2				49.18	53.03	55.89	58.36

4.4. Conclusion

The current chapter describes the utility of silane functionalized-GO as a reinforcing material for fabrication of HPUNC. The nanocomposites were successfully fabricated *in situ* with different loadings of Si-GO. The nanomaterial was found to be well dispersed and easily compatible with the polymer matrix. The study revealed that the nanocomposite displayed significant enhancements in mechanical properties and thermal properties. Interestingly, the nanocomposites displayed self healing ability and inherent surface hydrophobicity, depending upon nanomaterial loading. The advent of such multi-faceted material may be useful in creating high performance smart materials for potential applications.

References

[1] Thakur, S. and Hu, J. Polyurethane: a shape memory polymer (SMP). In Yilmaz, F., editor, *Aspects of Polyurethanes*, pages 53-54. IntechOpen, London, 2017.

[2] Karak, N. *Biobased Smart Polyurethane Nanocomposites: From Synthesis to Applications*. Royal Society of Chemistry, London, 2017.

[3] Roy, D., Cambre, J. N., and Sumerlin, B. S. Future perspectives and recent advances in stimuli-responsive materials. *Progress in Polymer Science*, 35(1):278-301, 2010.

[4] Yang, Y. and Urban, M. W. Self-healing polymeric materials. *Chemical Society Reviews*, 42(17):7446-7467, 2013.

[5] Ganesh, V. A., Raut, H. K., Nair, A. S., and Ramakrishna, S. A review on self-cleaning coatings. *Journal of Materials Chemistry*, 21(41):16304-16322, 2011.

[6] Habault, D., Zhang, H., and Zhao, Y. Light-triggered self-healing and shape-memory polymers. *Chemical Society Reviews*, 42(17):7244-7256, 2013.

[7] Chang, B., Zhang, B., and Sun, T. Smart polymers with special wettability. *Small*, 13(4):1-16, 2017.

[8] Zhong, N. and Post W. Self-repair of structural and functional composites with intrinsically self-healing polymer matrices: a review. *Composites Part A: Applied Science and Manufacturing*, 69:226-239, 2015.

[9] Yang, Y. and Urban, M. W. Self-healing polymeric materials. *Chemical Society Reviews*, 42(17):7446-7467, 2013.

[10] Kang, X., Zi, W. W., Xu, Z. G., and Zhang, H. L. Controlling the micro/nanostructure of self-cleaning polymer coating. *Applied Surface Science*, 253(22):8830-8834, 2007.

[11] Han, S. and Chun B. C. Preparation of polyurethane nanocomposites via covalent incorporation of functionalized graphene and its shape memory effect. *Composites Part A: Applied Science and Manufacturing*, 58:65-72, 2014.

[12] Kim, J. T., Kim, B. K., Kim, E. Y., Kwon, S. H., and Jeong, H. M. Synthesis and properties of near IR induced self-healable polyurethane/graphene nanocomposites. *European Polymer Journal*, 49(12):3889-3896, 2013.

[13] Thakur, S. and Karak, N. Green reduction of graphene oxide by aqueous phytoextracts. *Carbon*, 50(14):5331-5339, 2012.

[14] Lin, Y., Jin, J., and Song, M. Preparation and characterization of covalent polymer functionalized graphene oxide. *Journal of Materials Chemistry*, 21(10):3455-3461, 2011.

[15] Huang, J., Ding, S., Xiao, W., Peng, Y., Deng, S., and Zhang, N. 3-Aminopropyl-triethoxysilane functionalized graphene oxide: a highly efficient and recyclable catalyst for Knoevenagel condensation. *Catalysis Letters*, 145(4):1000-1007, 2015.

[16] Owens, D. K. and Wendt, R. C. Estimation of the surface free energy of polymers. *Journal of Applied Polymer Science*, 13(8):1741-1747, 1969.

[17] Król, P. and Król, B. Surface free energy of polyurethane coatings with improved hydrophobicity. *Colloid and Polymer Science*, 290(10):879-893, 2012.

[18] Yang, H., Li, F., Shan, C., Han, D., Zhang, Q., Niu, L., and Ivaska, A. Covalent functionalization of chemically converted graphene sheets via silane and its reinforcement. *Journal of Materials Chemistry*, 19(26):4632-4638, 2009.

[19] Pu, X., Zhang, H. B., Li, X., Gui, C., and Yu, Z. Z. Thermally conductive and electrically insulating epoxy nanocomposites with silica-coated graphene. *RSC Advances*, 4(29):15297-15303, 2014.

[20] Cui, P., Lee, J., Hwang, E., and Lee, H. One-pot reduction of graphene oxide at subzero temperatures. *Chemical Communications*, 47(45):12370-12372, 2011.

[21] Guimont, A., Beyou, E., Alcouffe, P., Martin, G., Sonntag, P., and Cassagnau, P. Synthesis and characterization of PDMS-grafted graphite oxide sheets. *Polymer*, 54(18):4830-4837, 2013.

[22] Tzounis, L., Contreras-Caceres, R., Schellkopf, L., Jehnichen, D., Fischer, D., Cai, C., Uhlmann, P., and Stamm M. Controlled growth of Ag nanoparticles decorated onto the surface of SiO_2 spheres: a nanohybrid system with combined SERS and catalytic properties. *RSC Advances*, 4(34):17846-17855, 2014.

[23] Paulose, S., Raghavan, R., and George, B. K. Graphite oxide–iron oxide nanocomposites as a new class of catalyst for the thermal decomposition of ammonium perchlorate. *RSC Advances*, 6(51):45977-45985, 2016.

[24] Thakur, S. and Karak, N. Bio-based tough hyperbranched polyurethane–graphene oxide nanocomposites as advanced shape memory materials. *RSC Advances*, 3(24):9476-9482, 2013.

[25] Bayan, R. and Karak, N. Renewable resource modified polyol derived aliphatic hyperbranched polyurethane as a biodegradable and UV-resistant smart material. *Polymer International*, 66(6):839-850, 2017.

[26] Deka, H. and Karak, N. Bio-based hyperbranched polyurethanes for surface coating applications. *Progress in Organic Coatings*, 66(3):192-198, 2009.

[27] Bayan, R. and Karak, N. Renewable resource derived aliphatic hyperbranched polyurethane/aluminium hydroxide–reduced graphene oxide nanocomposites as

robust, thermostable material with multi-stimuli responsive shape memory features. *New Journal of Chemistry*, 41(17):8781-8790, 2017.

[28] Chen, D., Zhu, H., and Liu, T. In situ thermal preparation of polyimide nanocomposite films containing functionalized graphene sheets. *ACS Applied Materials & Interfaces*, 2(12):3702-3708, 2010.

[29] Thakur, S., Barua, S., and Karak, N. Self-healable castor oil based tough smart hyperbranched polyurethane nanocomposite with antimicrobial attributes. *RSC Advances*, 5(3):2167-2176, 2015.

[30] Wu, C., Huang, X., Wang, G., Wu, X., Yang, K., Li, S., and Jiang, P. Hyperbranched-polymer functionalization of graphene sheets for enhanced mechanical and dielectric properties of polyurethane composites. *Journal of Materials Chemistry*, 22(14):7010-7019, 2012.

[31] Thakur, S. and Karak, N. Ultratough, ductile, castor oil-based, hyperbranched, polyurethane nanocomposite using functionalized reduced graphene oxide. *ACS Sustainable Chemistry & Engineering*, 2(5):1195-1202, 2014.

[32] Song, P., Cao, Z., Cai, Y., Zhao, L., Fang, Z., and Fu, S. Fabrication of exfoliated graphene-based polypropylene nanocomposites with enhanced mechanical and thermal properties. *Polymer*, 52(18):4001-4010, 2011.

[33] Park J. H., Dao, T. D., Lee, H. I., Jeong, H. M., and Kim, B. K. Properties of graphene/shape memory thermoplastic polyurethane composites actuating by various methods. *Materials*, 7(3):1520-1538, 2014.

[34] Zhang, L., Jiao, H., Jiu, H., Chang, J., Zhang, S., and Zhao, Y. Thermal, mechanical and electrical properties of polyurethane/(3-aminopropyl)triethoxysilane functionalized graphene/epoxy resin interpenetrating shape memory polymer composites. *Composites Part A: Applied Science and Manufacturing*, 90:286-295, 2016.

[35] Parkin, I. P. and Palgrave, R. G. Self-cleaning coatings. *Journal of Materials Chemistry*, 15(17):1689-1695, 2005.

[36] Fürstner, R., Barthlott, W., Neinhuis, C., and Walzel, P. Wetting and self-cleaning properties of artificial superhydrophobic surfaces. *Langmuir*, 21(3):956-961, 2005.